Structural, Nanomechanical, and Computational Characterization of d , l -Cyclic Peptide Assemblies

Structural, Nanomechanical and Computational Characterization of *D*,*L*-Cyclic Peptide Assemblies

Daniel J. Rubin[‡1,2], Shahrouz Amini[‡3,4], Feng Zhou[3], Haibin Su[3], Ali Miserez[3,4,5], *Neel S. Joshi[1,2]

[1]Harvard University, School of Engineering and Applied Sciences

[2]Wyss Institute for Biologically Inspired Engineering

[3]Nanyang Technological University, School of Materials Science and Engineering

[4]Nanyang Technological University, Center for Biomimetic Sensor Science

[5]Nanyang Technological University, School of Biological Sciences

[‡] These authors contributed equally to this work

* njoshi@seas.harvard.edu

ABSTRACT

The rigid geometry and tunable chemistry of *D*,*L*-cyclic peptides makes them an intriguing building-block for the rational design of nano- and microscale hierarchically structured materials. Herein, we utilize a combination of electron microscopy, nanomechanical characterization including depth sensing-based bending experiments, and molecular modeling methods to obtain the structural and mechanical characteristics of *cyclo*-[(Gln-*D*-Leu)$_4$] (QL4) assemblies. QL4 monomers assemble to form large, rod-like structures with diameters up to 2 μm and lengths of 10s to 100s of μm. Image analysis suggests that large assemblies are hierarchically organized from individual tubes that undergo bundling to form larger structures. With an elastic modulus of 11.3 ± 3.3 GPa, hardness of 387 ± 136 MPa and strength (bending) of 98 ± 19 MPa the peptide crystals are among the most robust known proteinaceous micro- and nano-fibers. The measured bending modulus of micron-scale fibrils (10.5 ± 0.9 GPa) is in the same range as the Young's modulus measured by nanoindentation indicating that the robust nanoscale network from which the assembly derives its properties is preserved at larger length-scales. Materials selection charts are used to demonstrate the particularly robust properties of QL4 including its specific flexural modulus in which it outperforms a number of biological proteinaceous and non-proteinaceous materials including collagen and enamel. The facile synthesis, high modulus, and low density of QL4 fibers indicate that they may find utility as a filler material in a variety of high efficiency, biocompatible composite materials.

KEYWORDS

Cyclic peptides; Supramolecular; Molecular dynamics; Elastic modulus; Amyloid; Nanoindentation

Research into the structure, chemistry and functionality of biomaterials has accelerated in recent years with the goal of creating environmentally benign materials that have optimized physical and mechanical properties.[1] Many of these materials (*e.g.* silks,[2,3] collagens[4,5]) derive their properties from protein constituents,[6] which form specific secondary structures that assemble into higher order structures with robust yet efficient mechanical behavior.[7] Another class of proteinaceous materials, amyloid fibrils, are particularly interesting because they can be formed from many different protein sequences.[8] Amyloids were first studied in conjunction with neurodegenerative diseases such as Alzheimers,[9] but newly discovered amyloidogenic gene products are increasingly being associated with functional (as opposed to pathogenic) biological performance.[10] Amyloids are classified by their fibrillar structure in which β-strands associate to form an extended network of supramolecular β-sheets perpendicular to the long-axis of the fiber.[11] This structural motif is intriguing in that it is largely defined by the properties of the peptide backbone itself, namely the propensity for hydrogen bonding between carbonyl oxygen and amide hydrogen.[12] This allows a variety of different proteins, when subjected to various denaturing and assembly processes, to form amyloid-like structures.[13] These nanoscale fibrils, self-assembled from individual protein and peptide molecules, continue to grow and form robust fibers with hierarchical order. Indeed, the dense hydrogen bonding and ordered structure of amyloid materials renders them among the most robust known proteinaceous materials with experimentally determined Young's moduli at the nanoscale in the range of 2-4 GPa.[14,15] The combination of self-assembly, nanoscale order and high stiffness provides a breadth of

potential applications including light-harvesting,[16] carbon capture,[17] drug delivery,[18] and nanowire fabrication.[19]

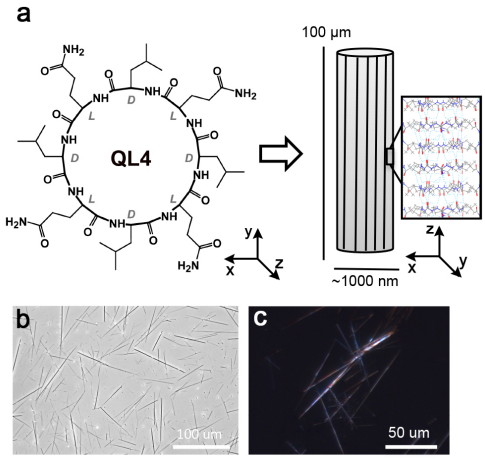

Figure 1. QL4 structure and assembly. (a) Chemical structure of QL4 and schematic of QL4 fiber. (b) Optical micrograph of QL4 fibers highlighting the size and rod-like structure. (c) Polarized light micrograph indicating that there is nanoscale order present in large QL4 structures.

D,*L*-cyclic peptides (DLCPs) share certain characteristics with amyloid fibrils including self-assembly, dense intermolecular hydrogen bonding along the peptide backbone, and chemical and mechanical stability. However, their molecular structure and geometry allow for an enhanced ability to chemically modify the monomers and to guide assembly.[20] The peptide cycles are composed of six to ten amino acids with alternating *D*- and *L*-stereochemistry, causing a planar geometry in which the amino acid side chains radiate from the center of the ring and the amide backbone is perpendicular to the plane of the ring. This geometrical arrangement promotes their assembly into high aspect ratio nano- and microstructures through β-sheet-like hydrogen bonding in which each ring sits flat on the surface of another ring (Figure 1a). Unlike linear amyloids in which β-sheets are able to slide with respect to one another,[21] DLCP assemblies are only able to stack directly atop each other. Depending on the sequence of the peptides, the nanotubes may also associate laterally

into bundles to create structures that can be microns in width and hundreds of microns in length.[22]

The assembly of cyclic peptides was first theorized by De Santis *et al*.[23] and later demonstrated using a pH sensitive peptide 8-mer that was found to assemble into large, micron-scale fibers.[20] As DLCPs are synthesized *via* common solid-state peptide synthesis methods[24], one has the freedom to explore limitless combinations of amino acids and post-synthetic modifications.[25] This versatility has been leveraged to study DLCPs in a variety of applications including structural antibiotics,[26] ion channels,[27] selective ion transporters,[28] and reinforcing agents.[29] Additional research has focused on the fundamental properties of cyclic peptides including the thermodynamics of assembly and the breadth of structural flexibility.[30] One area that remains largely unexplored is the utility of cyclic peptides as structural components of composite materials, perhaps because there is little information on the mechanical properties of DLCP structures themselves. While several computational analyses of DLCP structures indicate that they are quite stiff,[31-32] there have been no direct measurements of their mechanical properties. As amyloids represent some of the stiffest known protein-based materials, we hypothesized that the similarly structured DLCP assemblies would also exhibit high modulus and strength. The unusual ability of DLCPs to position functional groups precisely in space, coupled with their relatively straightforward synthesis, make them well suited to study the combined effects of geometry and sequence on mechanical properties. Such a study would provide essential information for downstream applications of DLCPs within medical devices and tissue scaffolds.

In this study we demonstrate that assemblies of the DLCP *cyclo*-[(Gln-*D*-Leu)$_4$], abbreviated here as QL4, are among the stiffest and strongest known peptide-based materials. This was accomplished through computational, structural and nanomechanical analyses including molecular dynamics simulations, electron microscopy, nanoindentation, and micro-

bending studies. QL4 was selected because it is known to form assemblies, herein referred to as fibers, that are large and stable enough to be probed with accessible nanomechanical probe tools. This particular DLCP has also been shown to increase the elastic modulus of polylactides when incorporated as the filler component of a composite fiber.[29] While previous attempts at molecular dynamics simulations have given clues regarding the elastic modulus of a DLCP assembly,[31] this study represents the first experimental characterization of the mechanical properties of DLCP fibers.

RESULTS AND DISCUSSION

QL4 was synthesized (Figure S1), dissolved in neat trifluoroacetic acid and incubated in the presence of milli-Q water in a closed vessel. Over the course of approximately 72 hours, QL4 assemblies formed at the surface of the solution and were visualized with an optical microscope in bright field mode (Figure 1b). Some QL4 fibers reach 100s of microns in length while maintaining nanoscale order, which is indicated by their birefringence demonstrated under cross-polarized light (Figure 1c). It is evident from the size of the structures that an individual fiber is composed of thousands of individual nanotubes assembling laterally. The hydrogen-bonded network is apparent through the specific shift in the Amide bands of the Raman and FT-IR spectra, which is similar to that of β-sheets[22,33] (Figure S2). SEM analysis of the QL4 fibers indicates that there are two classes of assembled structures, those which are not bundled and have diameters on the order of ~100 nm and those that are bundled and have diameters on the order of a few microns (Figure 2a). Present within the larger bundles are striations that indicate a bundle is composed of several ~100 nm assemblies. Furthermore, within larger bundles, one observes gaps in which fibers have broken free as is highlighted in Figure 2b, indicating that the ~100 nm assemblies are discrete elements in the larger bundle. We hypothesize that this bundling may occur naturally due to hydrophobic effects between the surfaces of QL4 assemblies in an increasingly aqueous

environment during the assembly process or, alternatively, may be a function of the evaporation necessary in sample preparation. High-resolution TEM micrographs of fibers show striations with thicknesses of approximately 2 nm along the long-axis of the fiber, providing evidence that the QL4 fibers are composed of individual DLCP nanotubes (Figure 2c and d). Taken together, this information suggests that there are three levels of hierarchy in a large QL4 assembly: Individual tube (~ 2 nm diameter), fiber (~ 100 nm diameter), and bundled fiber (~ 1 μm diameter) (Figure 2e). While it is possible to verify the existence of the fiber, and bundled fiber, we have not obtained evidence that individual QL4 tubes exist in solution. Prior work has shown that conjugation of polymers to the DLCP side chains can lead to stable assemblies of individual DLCP tubes,[28, 34] however, we have found that without modification, individual tubes continue to grow until a larger fiber or bundled fiber is formed.

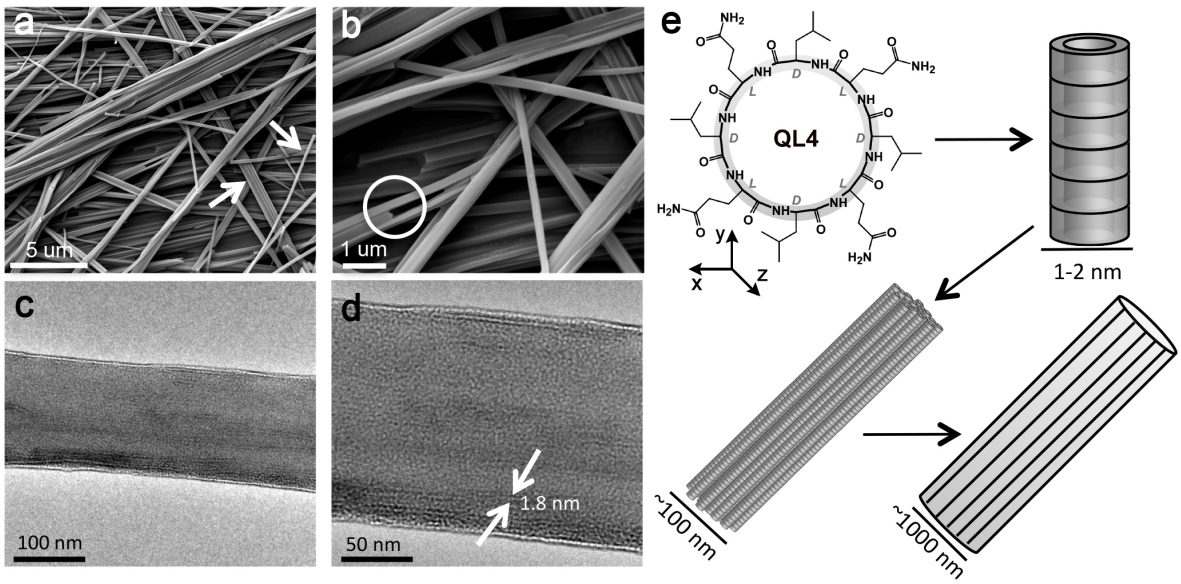

Figure 2. Structure of QL4 fibers. (a and b) Scanning electron micrographs highlight two major classes of fibers, single fibers (~100 nm diameter) and bundled fibers (~1 μm diameter). Bundled fibers have characteristic striations and points of fracture in which a single fiber was removed from the bundle. (c and d) High-resolution transmission electron micrographs indicate that single nanotubes (~2 nm diameter) are the building blocks of individual fibers. (e) A schematic representation of the hierarchical order present in a large, bundled QL4 fiber.

Through molecular dynamics simulations, we obtained a theoretically ideal structure for QL4 fibers and used this as a reference for both structural and mechanical analyses.

Along the longitudinal axis of assembly, QL4 monomers assemble through the creation of 12 hydrogen bonds, 8 along the peptide backbone and 4 mediated by glutamine sidechains, locking the monomers together with a spacing of 9.62 Å (Figure 3A) along the z-axis. Along the lateral axes of assembly (x and y) the fiber is most stable in a square-packed conformation with a unit cell spacing of 17.73 Å. In this orientation, glutamine residues and leucine residues provide interlaced hydrogen bond and hydrophobic interactions in the x-y plane. The density of the resultant peptide assembly is calculated to be 1000 kg/m^3. For further detail on the computational method and structure, please refer to the supplemental figures S3-S6. One can appreciate a key difference in the geometry of QL4 *versus* a typical amyloid in that for QL4, hydrophobic interactions are interdigitated with the hydrogen bonds in the lateral direction, while in a typical amyloid fibers, hydrogen bonds and hydrophobic interactions (or other –R group-mediated interactions) are present in two separate, orthogonal planes (Figure S7).[35] We hypothesize that these interlocking interactions are partially responsible for the solvent stability, large size, and general robustness of the assembled fibers- hydrogen bonds maintain their strength in the presence of nonpolar solvents while the interspersed leucine residues may act to prevent the ingress of polar solvents.

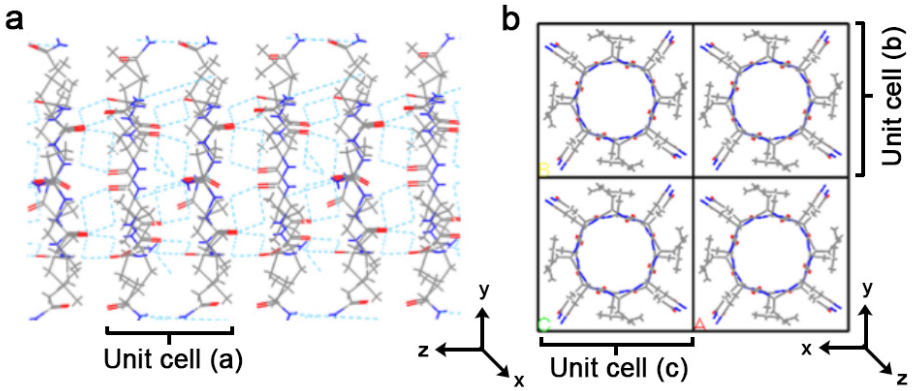

Figure 3. Molecular dynamics simulation of assembled QL4 structure. (a) A single nanotube assembles by forming anti-parallel β-sheet-like structures in which each monomer is connected to its neighbor *via* 8 hydrogen bonds along its peptide backbone. Amino acid side chains are free for lateral (x- and y- axis) and longitudinal (z-axis) interactions. (b) The lateral packing of individual nanotubes is governed by hydrogen bonding between glutamine side chains. This results in a stable, square packed structure in which glutamine-mediated hydrogen bonds interlace with hydrophobic leucine-leucine interactions.

We used the structural model to analyze the elastic modulus of the QL4 assembly in the X-, Y- and Z- axes as described in Figure 3. In the Z-axis, along the length of the tube, the theoretical modulus is 22.6 GPa, in line with the stiffest known protein-based materials.[8] In the X- and Y-axes, the modulus is approximately 2.7 GPa due to the decrease in hydrogen bonds per unit area within the structure (Figures S3-S6). It is worth noting that even in the comparatively compliant axes, our model suggests that QL4 assemblies possess a stiffness in the range of 2-4 GPa, equal to the measured value in amyloid fibers. Along the stiff axis, the theoretical modulus of 22.6 GPa is significantly higher than what has been measured at the nanoscale for amyloid or other protein-based fibrils.

The direct mechanical characterization of QL4 fibers was performed experimentally through both nanoindentation and micro-scale bending experiments, which were conducted using a depth-sensing nanoindenter. Both analyses were performed on large QL4 assemblies with widths ranging from 1-2 μm. In indentation studies, QL4 samples were deposited on a fused quartz substrate and probed with a cube corner diamond tip (Figure 4a). The position of each indent was accurately defined in the Scanning Probe Microscopy (SPM) mode and multiple indents were performed along the length of several fibers (Figure 4b). To confirm that indents occurred directly on the center of the fibers, FESEM micrographs were obtained after testing (Figure 4d). For each indent, modulus and hardness were calculated from the load *versus* depth curve generated with the indenter in load-controlled mode using the classical Oliver-Pharr analysis (Figure 4d-f and Figure S8). The average elastic modulus and hardness of a large QL4 fiber were determined to be 11.3 ± 3.3 GPa and 387 ± 136 MPa, respectively. It is intriguing to note that the average modulus (measured perpendicular to the fiber axis) is significant larger than the computed moduli in the x and y directions (2.72 GPa). We attribute this discrepancy to two factors. First, the indentation stress field beneath the

indenter is complex and characterized by principal tensile stresses whose direction lay almost perpendicular to the direction of indentation,[36] namely along the fiber axis. Since the computed modulus along the fiber axis is high (22.6 GPa), the results may be a consequence of some peptide nanotube sustaining tensile stresses during indentation, resulting in a higher apparent modulus. Second these results may also be a result of the strong lateral interactions between the individual peptide nanotubes, leading to increased mechanical stability, a hypothesis that is also supported by the micro-bending experiments presented next. Despite the large size of the fibers tested here, the measured modulus and hardness of QL4 fibers are also significantly higher than those measured for individual amyloid fibers by AFM-based methods.

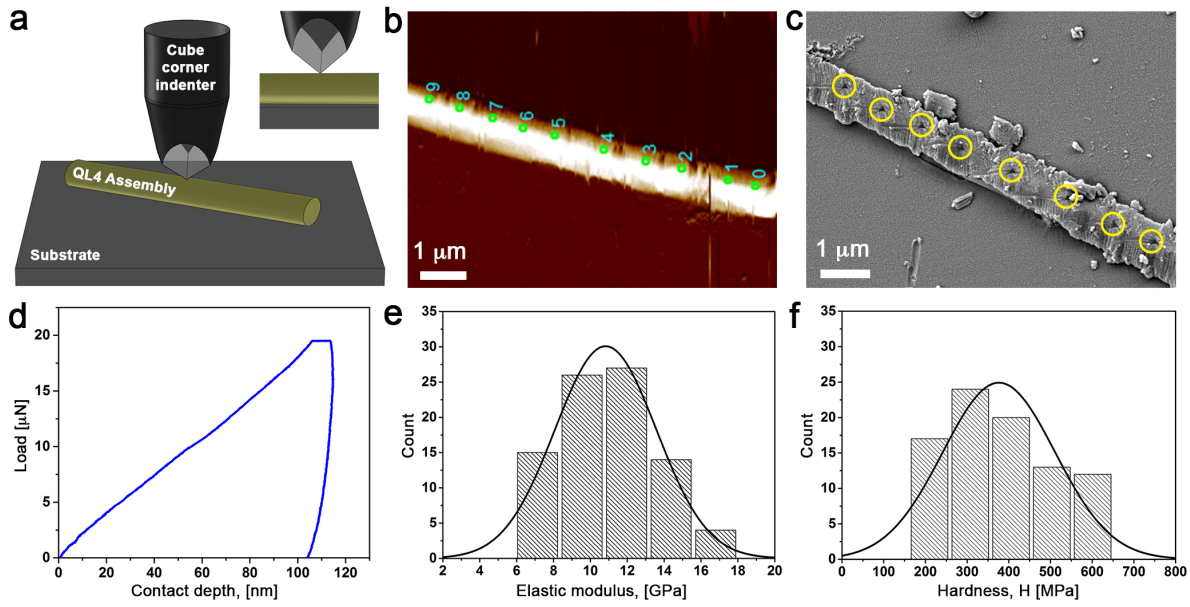

Figure 4. Nanoindentation of QL4 fibers. (a) QL4 fibers were deposited on a fused quartz substrate and probed directly with a cube corner indenter tip. (b) Scanning probe microscopy (SPM) was used to select multiple points to test along an individual fiber. (c) Residual indents were verified by FESEM analysis to confirm the spatial accuracy of each indent. (d) An individual load *versus* depth curve for a single indent. (e,f) The elastic modulus and hardness of over 100 individual indents were used to calculate the average values.

To elucidate the fracture strength of QL4 fibers and to gain a deeper understanding of the fiber modulus, fibers were subjected to a micro-scale bending analysis (Figure 5a). QL4

fibers were deposited on uncoated molybdenum TEM grids with 40 μm circular pores (Figure 5b). After locating individual fibers spanning pores in the grid, the fiber was bent, orthogonal to the long axis, by a cono-spherical tip with a 5 μm nominal radius. To confirm that fiber loading neither compressed the fiber nor bent the grid, the same force was applied to fibers on a flat surface and the measured displacement was negligible. Because the fibers are very long in comparison to the grid pore, and because the ends of the fiber did not appear to move during or after the experiment, we have used a clamped beam as a model for our calculations (Figure S9). The bending modulus and strength, 10.5 ± 0.9 GPa and 97.8 ± 18.8 MPa, respectively, were calculated from individual force *versus* displacement curves (Figure 5e and f). In the displacement curve, partial fracture is indicated by sudden decreases in the measured load (Figure 5d). We hypothesize that these micro-fractures occur as individual fibers within the larger bundle are broken and/or delaminated from one another (Figure 5c). It is worth noting that microscale modulus values *via* bending analysis are nearly identical to those obtained through nanoindentation perpendicular to the fiber axis. Unlike many other molecularly self-assembled systems, QL4 DLCPs are able to grow to such large sizes that direct nano- and micro-scale measurements can be obtained on the same samples and compared, providing an understanding of the mechanical properties across higher length scales.

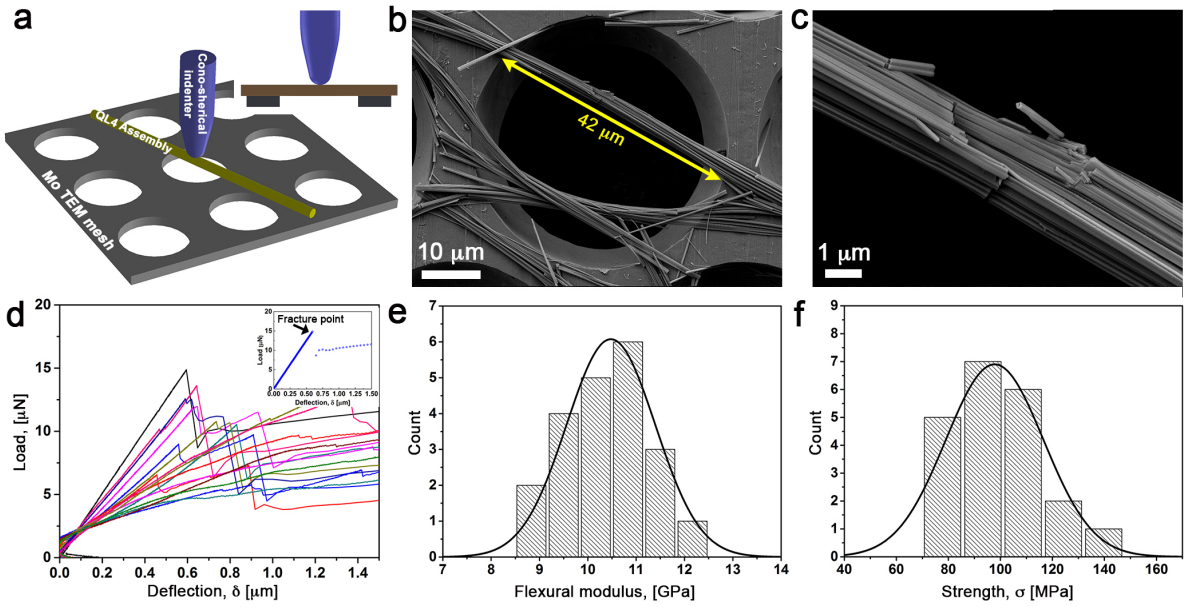

Figure 5. Bending analysis of QL4 fibers. (a) A 5 µm spherical tip was used to bend individual and bundled fibers over pores in a Mo grid. (b) A large QL4 bundled fiber bridges the pore of a Mo grid. (c) High magnification shows individual fracture events that occurred during the bending experiment. (d) Combined raw bending data for individual tubes. Curves exhibit a linear elastic region followed by a series of fracture events. A fracture point is presented at the inset image. (e-f) The bending modulus and fracture strength of QL4 fibers.

Prior bending analyses of other tube-based assemblies including single-walled carbon nanotube ropes and microtubules have shown that the shear modulus of the bundle is much weaker than the axial (Young's) modulus.[37,38] This is due primarily to a lack of inter-tube interaction within the bundle, which leads to bending and flexing as tubes slide with respect to one another. Conversely, QL4 fibers contain a dense network of inter-tube hydrogen bonds, mediated by glutamine side chains that act to stabilize each tube with respect to its neighbors (Figure S6). We suggest that these lateral interactions are directly responsible for the robust flexural and Young's moduli because they lead to more efficient load transfer between the tubes, which is also in line with the high modulus measured by nanoindentation. Indeed high load transfer will enhance the development of a continuum-like stress field beneath the indenter that results in regions of the fibers to be under tensile stresses, as discussed above. Furthermore these interactions contribute to the remarkably rigid, rod-like

morphology of QL4 fibers. The overall rigidity, characterized by the persistence length ($l_p = EI/k_bT$), where I is the moment of inertia of the fibers, is on the order of meters (assuming a circular cross-section), which explains the lack of any noticeable bending within the fibers observed to date. This brings to light an interesting lever with which one may be able to tune the properties of DLCP structures. By tuning the side chain chemistry of the individual DCLP monomer that composes the fiber, one may be able to tune the flexural modulus and control the general morphology and properties of the assembled fiber to be more rod-like or more flexible in nature. A summary of the mechanical results for both the computational and experimental analyses is presented in Figure 6.

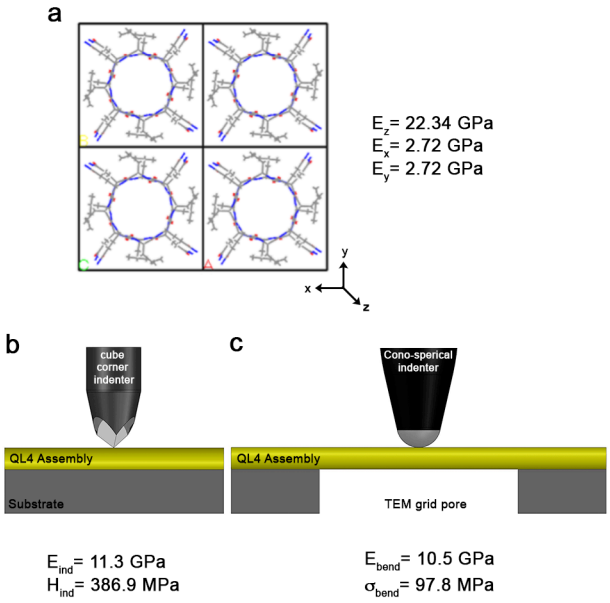

Figure 6. Summary of mechanical analyses and deformation modes. (a) Molecular dynamics simulations suggest that the elastic modulus parallel to the long axis of a fiber is 22.34 GPa. In the 'weak' directions, the elastic modulus is 2.72 GPa. (b) Nanoindentation experiments and (c) bending experiments confirm a ~11 GPa modulus.

In order to place the modulus and strength of QL4 within the context of other natural and synthetic materials, we have constructed two material selection charts (Ashby plots): one modulus *vs*. density plot (Figure 7a), with the density inferred from the computational

modeling, and one modulus *vs*. strength plot (Figure 7b). A subset of the data on the plots is also tabulated in numerical form in the Supplementary Information (Figure S10). Guidelines drawn on the modulus *vs*. density plot allows one to compare the specific performance of materials in tension (given by E/ρ) or in bending (given by $E^{1/2}/\rho$).[7, 39] One sees that the efficiency of QL4 fibers in tension outpaces a variety of materials, including collagen, tendon, and cancellous and compact bone. The material outperformance is more significant when considering the material efficiency in bending, where QL4 fibers also outperform enamel and even steel. The relatively facile synthesis, high aspect ratio, high modulus, and low density of QL4 fibers indicate that they may find utility as a filler material in a variety of high efficiency, biocompatible composite materials.

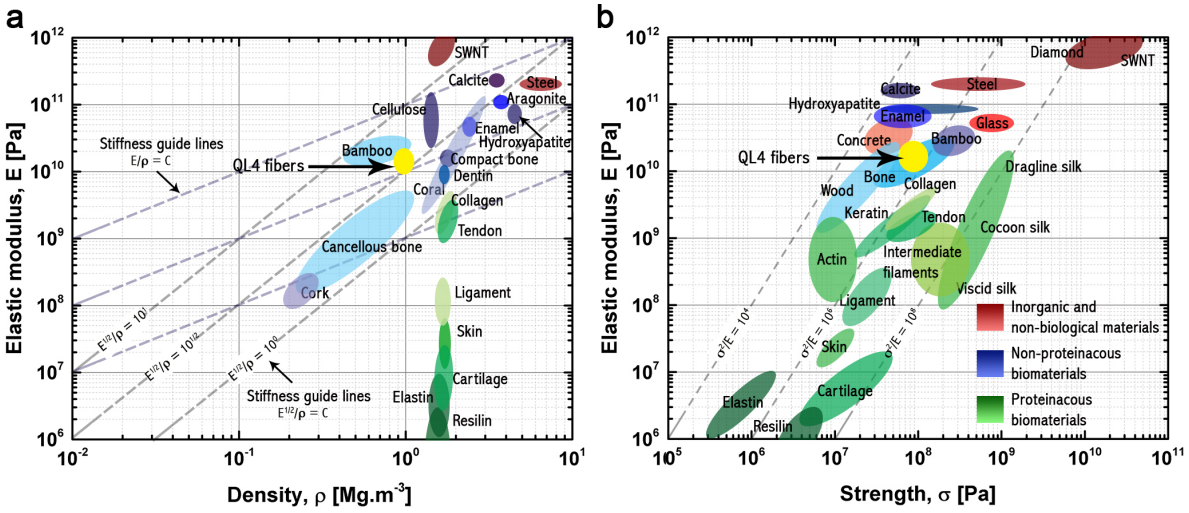

Figure 7. Comparison of materials properties modified from references 7 and 37. (a) Young's modulus *versus* density of a variety of materials. Tie lines represent the efficiency of materials in tension (E/ρ) and bending ($E^{1/2}/\rho$). QL4 fibers are among the stiffest known protein-based materials and surpass collagen, tendon, and compact bone in density-adjusted flexural modulus. (b) Young's modulus *versus* strength for a variety of materials. Tie lines represent the ability of a material to store elastic energy (σ_f^2/E). In comparing the stiffness and strength, it is evident that QL4 fibers exhibit similar behavior to bone and that their modulus is on par with the stiffest known proteinaceous materials including spider dragline silk.

The stiffness vs. strength selection chart of QL4 (Fig. 7b), together with the materials index σ_f^2/E (guidelines with slope of 2) allows one to compare the materials performance in terms of their ability to store elastic energy prior to fracture.[7, 39] In both stiffness and strength,

QL4 fibers are most directly comparable to bone. The stiffness of QL4 fibers exceed that of all but the most robust known proteinaceous materials such as spider dragline silk. Although the elastic energy to failure of silks is superior, as evidenced by their location along the far-right guideline in Figure 7b, QL4 fibers exhibit a performance metric on par with commonly known biological materials such as collagen, tendon and keratin. Perhaps unexpectedly, Figure 7a and 7b support the claim that the mechanical response of QL4 fibers is more similar to 'light' bone than to other protein based materials.

CONCLUSION

Our multi-scale mechanical analysis of QL4 fibers by nanoindentation and micro-bending demonstrates that DLCP assemblies are comparable to the most robust known protein and peptide materials. Indeed, the properties exceed those of amyloid fibrils and are on par with those of silks, suckerins,[40,41] and diphenylalanine nanotubes,[42] the most robust known self-assembling peptide based materials. Furthermore, they maintain those properties even at the micron length scale. This is a noteworthy feature given that the larger scale assembly is not stabilized by covalent, electrostatic, or coordination bonds between the individual monomers. In terms of stiffness and strength, QL4 is similar to bone, despite being roughly half the density. We hypothesize that the stiffness in both indentation and flexural deformation modes is supported by the rigid geometry as well as the density of hydrogen bonds in the lateral and longitudinal axes within the fibers, leading to the high persistence length and rod-like morphologies observed. Looking forward, there are a number of parameters worth considering in order to modulate the properties of the assembled fiber including modifying the primary sequence, inducing covalent linkages, and assembling structures *in situ* within other materials to form nano-composites. The simple synthesis, ease of modification, potential for biocompatibility, rod-like morphology, and robust mechanical properties of DLCPs make them a promising class of peptides for further exploration in

materials science, chemistry and biology, particularly as mechanical fillers in low-weight, high-stiffness composite materials.

Methods

Chemicals and Reagents Acetone, dichloromethane, dimethylformamide, diisopropylamine, and piperidine were purchased from Sigma Aldrich. Dichloromethane and dimethylformamide were dried over molecular sieves. The following chemicals were used as provided: Acetone, trifluoroacetic acid, 2-(1*H*-benzotriazol-1-yl)-1,1,3,3-tetramethyluronium hexafluorophosphate (HBTU), and (benzotriazol-1-yl-oxytripyrrolidinophosphonium hexafluorophosphate) (PyBOP) (Sigma Aldrich). All amino acids and Rink Amide-MBHA resin were purchased from AAPPTEC, Louisville Kentucky.

Cyclic Peptide Synthesis and Assembly *D*-,*L*-cyclic peptides were synthesized in accordance with the procedure of McMurray.[24] Fmoc-Glu-OAll was coupled to a Rink Amide-MBHA resin through the side-chain carboxylate. When cleaved, this residue is converted to a Gln. Standard Fmoc synthesis produced an uncyclized 8-mer which was cyclized through a PyBop assisted coupling reaction. Peptides were cleaved from the resin with 95% TFA, 2.5% water and 2.5% triisopropylsilane. To isolate the peptide, the TFA solution was concentrated by evaporation and dropped into cold diethyl ether causing precipitation. The mixture was centrifuged, resuspended in TFA and precipitated again to increase purity. Cyclic peptide identity was verified by liquid chromatography electrospray ionization mass spectroscopy. Self-assembly was achieved by dissolving 2.5 mg/ml of QL4 in a mixture of 60% TFA and 40% water. The assembly occurred in a glass vial over 48-72 hours at which point microcrystals could be seen by eye. Assemblies were harvested by diluting the assembly with a mixture of acetone and dichloromethane and pelleting the crystals by centrifugation.

Light Microscopy QL4 samples were deposited on glass slides and viewed on a Zeiss Axio Observer inverted microscope. Assembled fibers were suspended in water, deposited on a slide, allowed to dry and were viewed under both brightfield and cross-polarized light conditions.

Field emission scanning electron microscopy of QL4 assemblies QL4 samples were deposited on a quartz substrate and sputter coated to a projected thickness of ~5 nm. All samples were sputter-coated with Au/Pd and then imaged on a Zeiss FE-SEMSupra55VP (Carl Zeiss, Oberkochen, DE) in SE2 mode. After indentation observations were performed using a FESEM (JEOL, 7600 F) at a 5 kV accelerating voltage using a lower secondary electron detector (LEI) to prevent surface charging.

Transmission electron microscopy of QL4 assemblies A suspension of QL4 assemblies in water was spotted on a quantifoil TEM grid, wicked away, and stained with uranyl acetate. Sample was viewed on a JEOL2100 TEM at 200kV. For higher resolution images, spots were selected in which the assembly was overlapping a pore in the quantifoil.

Molecular dynamics simulation of QL4 structure and stiffness We employed the COMPASS force field (Condensed-phase Optimized Molecular Potentials for Atomistic Simulation Studies) - developed by H. Sun,[43] to optimize the geometry and calculate the energy of all molecules. The COMPASS force field is based on state-of-the-art ab *initio* and empirical parametrization techniques. The valence parameters and atomic partial charges were supported by ab *initio* data, and the van der Waals (vdW) parameters were derived by fitting the experimental data of cohesive energies and equilibrium densities. For more details, please refer to the supplemental information.

Nanoindentation and Bending of QL4 assemblies QL4 assemblies were suspended in water and dropped onto a fused-quartz substrate. The droplet was wicked away, leaving

numerous assemblies along the surface. A Triboindenter TI-950 Nanomechanical tester (Hysitron, Minneapolis, MN, USA) equipped with a 2D standard transducer and a 50 nm cube-corner tip was used to do SPM imaging and indent along the length of individual structures. The tip was calibrated using a standard fused quartz sample. For bending studies, QL4 assemblies were deposited on a Mo TEM grid with circular pores of 40 μm diameter. Assemblies overlapping pores were bent using a 5 μm cono-spherical indenter tip. The force and displacement curves were used to identify the modulus and strength as well as the nature of fracture of the material.

ASSOCIATED CONTENT

Supporting Information

The Supporting Information Available: Diagram and mass spectrometric characterization of QL4, FTIR and Raman spectra, detailed description of molecular dynamics approach, schematic of *β*-sheet and DLCP structures, description of nanoindentation and bending. This material is available free of charge *via* the Internet at http://pubs.acs.org.

AUTHOR INFORMATION

Corresponding Author

* Mailing address: Pierce Hall 29 Oxford St. Cambridge, MA 02138; tel: 617-432-7730; e-mail: njoshi@seas.harvard.edu

ACKNOWLEGEMENT

N.S.J. acknowledges funding support from the Harvard MRSEC, the Army Research Office STIR program under award no. ARO-167836, the IMI Program of the National Science Foundation under award no. DMR 08-43934, and the Center for Nanoscale Systems (CNS) at Harvard University, a member of the National Nanotechnology Infrastructure Network (NNIN), which is supported by the National Science Foundation under NSF award no. ECS-0335765. A.M thanks the support of the Singapore National Research Foundation (NRF) though a NRF Fellowship.

REFERENCES

1. Zhao, N.; Wang, Z.; Cai, C.; Shen, H.; Liang, F.; Wang, D.; Wang, C.; Zhu, T.; Guo, J.; Wang, Y., *et al*., Bioinspired Materials: From Low to High Dimensional Structure. *Adv. Mater*. **2014,** *26*, 6994-7017.
2. Winkler, S.; Kaplan, D. L., Molecular Biology of Spider Silk. *Rev. Mol. Biotechnol*. **2000,** *74*, 85-93.
3. Tao, H.; Kaplan, D. L.; Omenetto, F. G., Silk Materials--a Road to Sustainable High Technology. *Adv. Mater*. **2012,** *24*, 2824-2837.
4. van der Rest, M.; Garrone, R., Collagen Family of Proteins. *FASEB J*. **1991,** *5*, 2814-2823.
5. Fratzl, P., *Collagen: Structure and Mechanics*. Springer: 2008.
6. Hu, X.; Cebe, P.; Weiss, A. S.; Omenetto, F.; Kaplan, D. L., Protein-Based Composite Materials. *Materials Today* **2012**.
7. Wegst, U. G. K.; Ashby, M. F., The Mechanical Efficiency of Natural Materials. *Philos. Mag*. **2004,** *84*, 2167-2186.
8. Knowles, T. P. J.; Buehler, M. J., Nanomechanics of Functional and Pathological Amyloid Materials. *Nat. Nanotechnol*. **2011,** *6*, 469-479.
9. Selkoe, D. J., Alzheimer's Disease: Genes, Proteins, and Therapy. *Physiol. Rev*. **2001,** *81*, 741-766.
10. Zganec, M.; Zerovnik, E., Amyloid Fibrils Compared to Peptide Nanotubes. *Biochim. Biophys. Acta* **2014,** *1840*, 2944-2952.
11. Chiti, F.; Dobson, C. M., Protein Misfolding, Functional Amyloid, and Human Disease. *Annu. Rev. Biochem*. **2006,** *75*, 333-366.
12. Dobson, C. M., Protein Folding and Misfolding. *Nature* **2003,** *426*, 884-890.
13. Adamcik, J.; Jung, J.-M.; Flakowski, J.; De Los Rios, P.; Dietler, G.; Mezzenga, R., Understanding Amyloid Aggregation by Statistical Analysis of Atomic Force Microscopy Images. *Nat. Nanotechnol*. **2010,** *5*, 423-428.
14. Smith, J. F.; Knowles, T. P. J.; Dobson, C. M.; Macphee, C. E.; Welland, M. E., Characterization of the Nanoscale Properties of Individual Amyloid Fibrils. *Proc. Natl. Acad. Sci*. **2006,** *103*, 15806-15811.
15. Adamcik, J.; Lara, C.; Usov, I.; Jeong, J. S.; Ruggeri, F. S.; Dietler, G.; Lashuel, H. A.; Hamley, I. W.; Mezzenga, R., Measurement of Intrinsic Properties of Amyloid Fibrils by the Peak Force Qnm Method. *Nanoscale* **2012,** *4*, 4426-4429.
16. Channon, K. J.; Devlin, G. L.; Macphee, C. E., Efficient Energy Transfer within Self-Assembling Peptide Fibers: A Route to Light-Harvesting Nanomaterials. *J. Am. Chem. Soc*. **2009,** *131*, 12520-12521.
17. Li, D.; Furukawa, H.; Deng, H.; Liu, C.; Yaghi, O. M.; Eisenberg, D. S., Designed Amyloid Fibers as Materials for Selective Carbon Dioxide Capture. *Proc. Natl. Acad. Sci*. **2014,** *111*, 191-196.
18. Maji, S. K.; Schubert, D.; Rivier, C.; Lee, S.; Rivier, J. E.; Riek, R., Amyloid as a Depot for the Formulation of Long-Acting Drugs. *PLoS Biol*. **2008,** *6*, e17.
19. Reches, M.; Gazit, E., Casting Metal Nanowires within Discrete Self-Assembled Peptide Nanotubes. *Science* **2003,** *300*, 625-627.
20. Ghadiri, M.; Granja, J.; Milligan, R.; McRee, D.; Khazanovich, N., Self-Assembling Organic Nanotubes Based on a Cyclic Peptide Architecture. *Nature* **1994,** *372*, 709-709.
21. Keten, S.; Xu, Z.; Ihle, B.; Buehler, M. J., Nanoconfinement Controls Stiffness, Strength and Mechanical Toughness of Beta-Sheet Crystals in Silk. *Nat. Mater*. **2010,** *9*, 359-367.
22. Hartgerink, J. D.; Granja, J. R.; Milligan, R. A.; Ghadiri, M. R., Self-Assembling Peptide Nanotubes. *J. Am. Chem. Soc*. **1996,** *118*, 43-50.

23. De Santis, P.; Morosetti, S.; Rizzo, R., Conformational Analysis of Regular Enantiomeric Sequences. *Macromolecules* **1974,** *7*, 52-58.
24. McMurray, J. S., Solid Phase Synthesis of a Cyclic Peptide Using Fmoc Chemistry. *Tetrahedron Lett*. **1991,** *32*, 7679-7682.
25. Hourani, R.; Zhang, C.; van der Weegen, R.; Ruiz, L.; Li, C.; Keten, S.; Helms, B. A.; Xu, T., Processable Cyclic Peptide Nanotubes with Tunable Interiors. *J. Am. Chem. Soc*. **2011,** *133*, 15296-9.
26. Fernandez-Lopez, S.; Kim, H. S.; Choi, E. C.; Delgado, M.; Granja, J. R.; Khasanov, A.; Kraehenbuehl, K.; Long, G.; Weinberger, D. A.; Wilcoxen, K. M., *et al*., Antibacterial Agents Based on the Cyclic D,L-Alpha-Peptide Architecture. *Nature* **2001,** *412*, 452-455.
27. Motesharei, K.; Ghadiri, M. R., Diffusion-Limited Size-Selective Ion Sensing Based on Sam-Supported Peptide Nanotubes. *J. Am. Chem. Soc*. **1997,** *119*, 11306-11312.
28. Xu, T.; Zhao, N.; Ren, F.; Hourani, R.; Lee, M. T.; Shu, J. Y.; Mao, S.; Helms, B. A., Subnanometer Porous Thin Films by the Co-Assembly of Nanotube Subunits and Block Copolymers. *ACS Nano* **2011,** *5*, 1376-1384.
29. Rubin, D. J.; Nia, H. T.; Desire, T.; Nguyen, P. Q.; Gevelber, M.; Ortiz, C.; Joshi, N. S., Mechanical Reinforcement of Polymeric Fibers through Peptide Nanotube Incorporation. *Biomacromolecules* **2013,** *14*, 3370-3375.
30. Chapman, R.; Danial, M.; Koh, M. L.; Jolliffe, K. A.; Perrier, S., Design and Properties of Functional Nanotubes from the Self-Assembly of Cyclic Peptide Templates. *Chem. Soc. Rev*. **2012,** *41*, 6023-6041.
31. Diaz, J. A. C.; Çağin, T., Thermo-Mechanical Stability and Strength of Peptide Nanostructures from Molecular Dynamics: Self-Assembled Cyclic Peptide Nanotubes. *Nanotechnology* **2010,** *21*, 115703.
32. Ruiz, L.; VonAchen, P.; Lazzara, T. D.; Xu, T.; Keten, S., Persistence Length and Stochastic Fragmentation of Supramolecular Nanotubes under Mechanical Force. *Nanotechnology* **2013,** *24*, 195103.
33. Movasaghi, Z.; Rehman, S.; Rehman, I. U., Raman Spectroscopy of Biological Tissues. *Appl. Spectrosc. Rev*. **2007,** *42*, 493-541.
34. Couet, J.; Samuel, J. D. J. S.; Kopyshev, A.; Santer, S.; Biesalski, M., Peptide-Polymer Hybrid Nanotubes. *Angew. Chem., Int. Ed*. **2005,** *44*, 3297-3301.
35. Volpatti, L. R.; Knowles, T., Polymer Physics Inspired Approaches for the Study of the Mechanical Properties of Amyloid Fibrils. *Journal of Polymer Science Part B: …* **2014**.
36. Fischer-Cripps, A. C., *Nanoindentation*. Springer: 2011; Vol. 1.
37. Kis, A.; Kasas, S.; Babić, B.; Kulik, A.; Benoît, W.; Briggs, G.; Schönenberger, C.; Catsicas, S.; Forró, L., Nanomechanics of Microtubules. *Phys. Rev. Lett*. **2002,** *89*, 248101.
38. Salvetat, J. P.; Briggs, G.; Bonard, J. M.; Bacsa, R. R., Elastic and Shear Moduli of Single-Walled Carbon Nanotube Ropes. *Phys. Rev. Lett*. **1999**.
39. Ashby, M. F.; Gibson, L. J.; Wegst, U.; Olive, R., The Mechanical Properties of Natural Materials. I. Material Property Charts. *Proc. R. Soc. London, A* **1995,** *450*, 123-140.
40. Guerette, P. A.; Hoon, S.; Ding, D.; Amini, S.; Masic, A.; Ravi, V.; Venkatesh, B.; Weaver, J. C.; Miserez, A., Nanoconfined B-Sheets Mechanically Reinforce the Supra-Biomolecular Network of Robust Squid Sucker Ring Teeth. *ACS Nano* **2014,** *8*, 7170-7179.
41. Guerette, P. A.; Hoon, S.; Seow, Y.; Raida, M.; Masic, A.; Wong, F. T.; Ho, V. H. B.; Kong, K. W.; Demirel, M. C.; Pena-Francesch, A., *et al*., Accelerating the Design of Biomimetic Materials by Integrating Rna-Seq with Proteomics and Materials Science. *Nat. Biotechnol*. **2013,** *31*, 908-915.

42. Kol, N.; Adler-Abramovich, L.; Barlam, D.; Shneck, R. Z.; Gazit, E.; Rousso, I., Self-Assembled Peptide Nanotubes Are Uniquely Rigid Bioinspired Supramolecular Structures. *Nano Lett*. **2005,** *5*, 1343-1346.
43. Sun, H., Compass: An Ab Initio Force-Field Optimized for Condensed-Phase Applications Overview with Details on Alkane and Benzene Compounds. *J. Phys. Chem. B* **1998,** *102*, 7338-7364.

TABLE OF CONTENTS FIGURE

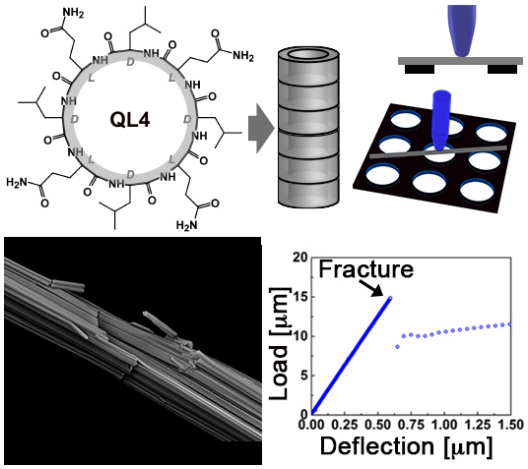

Structural, Nanomechanical and Computational Characterization of D,L-Cyclic Peptide Assemblies

Daniel J. Rubin[‡1,2], Shahrouz Amini[‡3,4], Feng Zhou[3], Haibin Su[3], Ali Miserez[3,4,5], *Neel S. Joshi[1,2]

[1]Harvard University, School of Engineering and Applied Sciences

[2]Wyss Institute for Biologically Inspired Engineering

[3]Nanyang Technological University, School of Materials Science and Engineering

[4]Nanyang Technological University, Center for Biomimetic Sensor Science

[5]Nanyang Technological University, School of Biological Sciences

[‡] These authors contributed equally to this work

* njoshi@seas.harvard.edu

Figure S1:

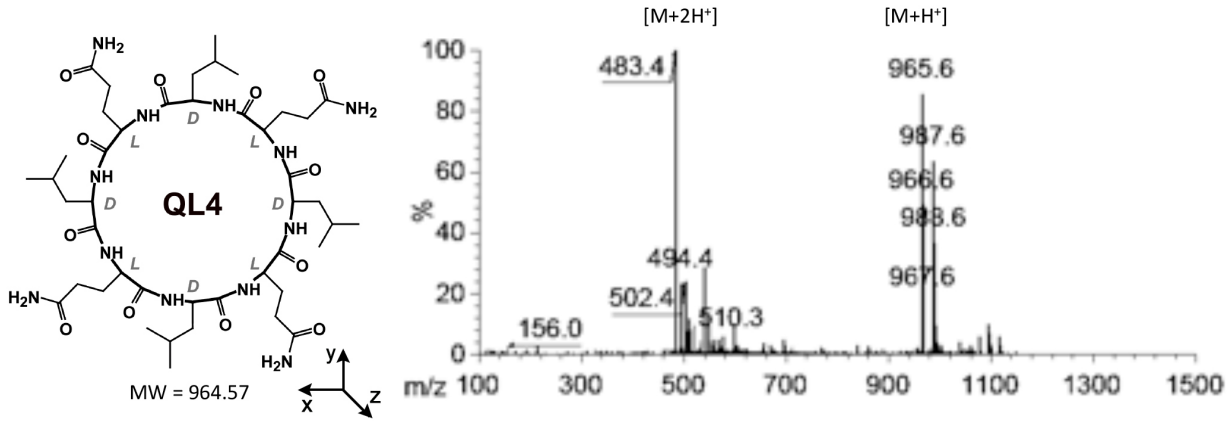

Figure S1: Analysis of cyclo-[$(QL)_4$]. [left] QL4 structure and molecular weight. [right] A singly charged [$M+H^+$] QL4 ion is visible at 965.6 m/z and the doubly charged [$M+2H^+$] is visible at 483.4 m/z.

Figure S2:

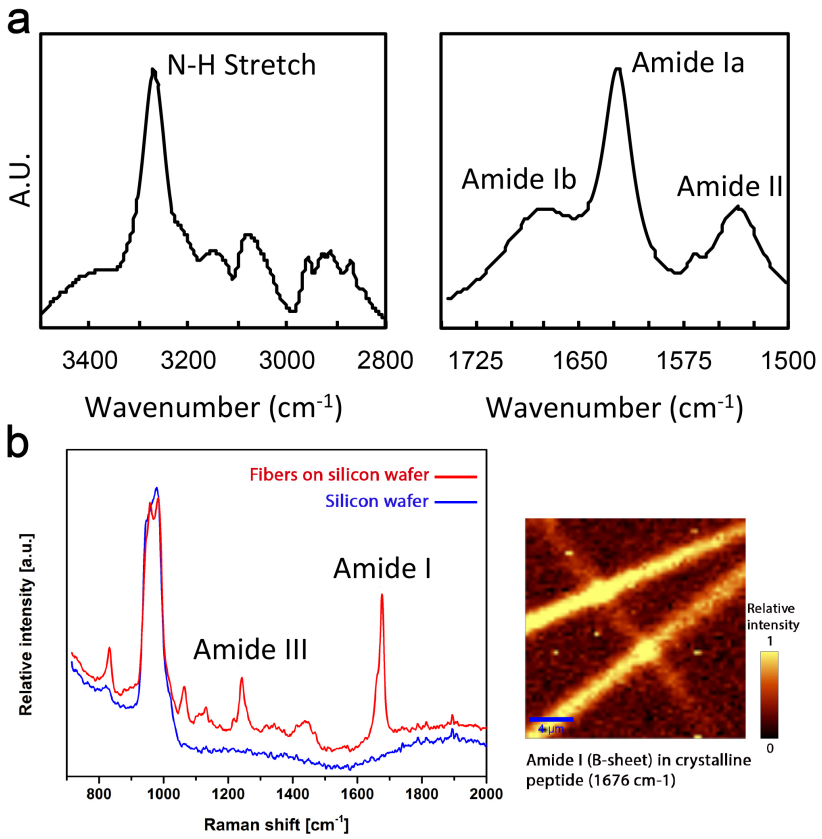

Figure S2: FTIR and Raman Spectroscopy of QL4 Crystals. (a) [left] The characteristic N-H stretching frequency at 3278 cm^{-1} indicates a hydrogen bonded network with an average intersubunit distance of 4.7-4.8 Å,[1] providing evidence that QL4 fibers are composed of peptide nanotubes. [right] In concordance with prior literature, Amide 1a, Amide 1b, and Amide II are present at 1629 cm^{-1}, 1688 cm^{-1}, and 1540 cm^{-1}, respectively.[1] (b) [left] Characteristic Raman spectra of an assembled QL4 fiber. Strong peaks at 1242 cm^{-1} and 1676 cm^{-1} correspond to Amide III and Amide I beta sheet signals, respectively.[2] [right] Raman map of peptide assemblies obtained by monitoring the intensity of the amide peak at 1676 cm^{-1}.

Method for modeling peptide behavior

In this paper, we employed the COMPASS force field (Condensed-phase Optimized Molecular Potentials for Atomistic Simulation Studies) - developed by H. Sun[3], to optimize the geometry and calculate the energy of all molecules. The COMPASS force field is based on state-of-the-art ab *initio* and empirical parametrization techniques. The valence parameters and atomic partial charges were supported by ab *initio* data, and the van der Waals (vdW) parameters were derived by fitting the experimental data of cohesive energies and equilibrium densities.

The convergence tolerance is $2x10^{-5}$ kcal/mol for the energy, 0.001 kcal/mol/Å for the force, 0.001 GPa for the stress and 10^{-5} Å for the displacement. The Ewald method is used for calculating the electrostatic and the van der Waals terms. The accuracy is 10^{-5} kcal/mol. The repulsive cutoff is 6 Å for the van der Waals term. For the periodical structure, the box vectors are also optimized together with the molecules. The Mechanical Properties are calculated by applying strain using static approach. The elastic constants were calculated from a polynomial fit to the calculated stress–strain relation.

Elastic constants of cyclic peptide nanotubes

Table 1:

Cij of Model1	(GPa)	Cij of Model2	(GPa)
C11	2.72	C11	4.43
C22	2.72	C22	1.36
C33	22.62	C33	20.21

Table 1: Elastic constants of cyclic peptide nanotubes.

The lattice constants are calculated as a= 17.73 Å b= 17.73 Å c= 9.62 Å at the optimized structure. The elastic constants are reported in Table 1. The value of *C*33 is the highest since the cyclic peptides are assembled by strong H-bonds along the *z* direction. This is the major source

for stabilizing the peptide in the nanotube form. The values of $C11$ and $C22$ are smaller compared with the $C33$ coefficient, which is due to the decrease in hydrogen bond density as well as the comparatively weaker interactions, such as van der Waals and electrostatic type, among cyclic peptides in the x-y plane. Hence, the anisotropy of the system is manifested by the more rigid character in the *z* direction. When taking the Cii (i=1,2,3) as the approximate Young's moduli, the data in Table 1 are in good agreement with previously reported results for similar peptide nanotubes and protein crystalline systems[4,1] and also with the experimental data measured in this work.

The hydrogen bonds network forms axial periodicities

Figure S3:

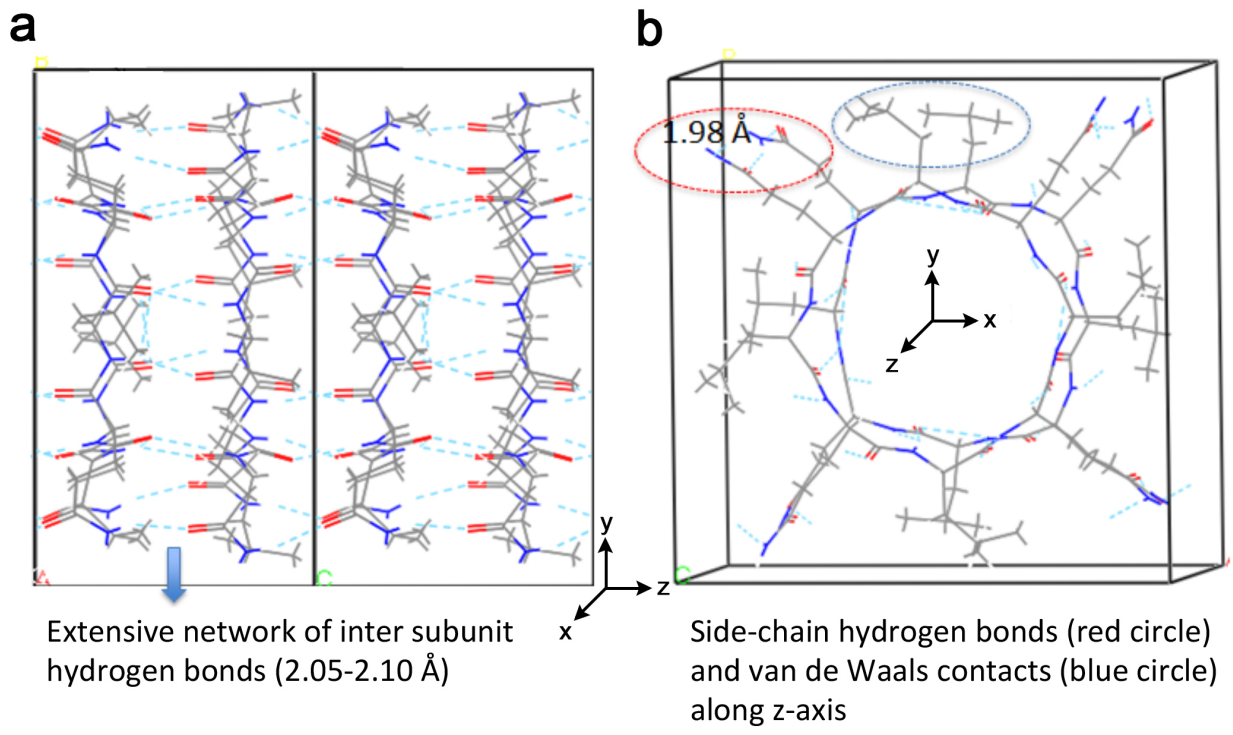

Figure S3: The hygrogen bonds between the backbones (a) and sidechains (b) in the Peptide nanostructures (Model 1)

As shown in figure 1, the hydrogen bonded peptide subunits stacked tightly in an ideal antiparallel *β*-sheet-like arrangement. Along z-axis there are eight hydrogen bonds of 2.05-2.10 Å between the backbone of subunits and four hydrogen bonds of 1.98 Å between the sidechains of subunits, this supports the presence of the highly ordered axial periodicities (along the *z direction*).

Figure S4:

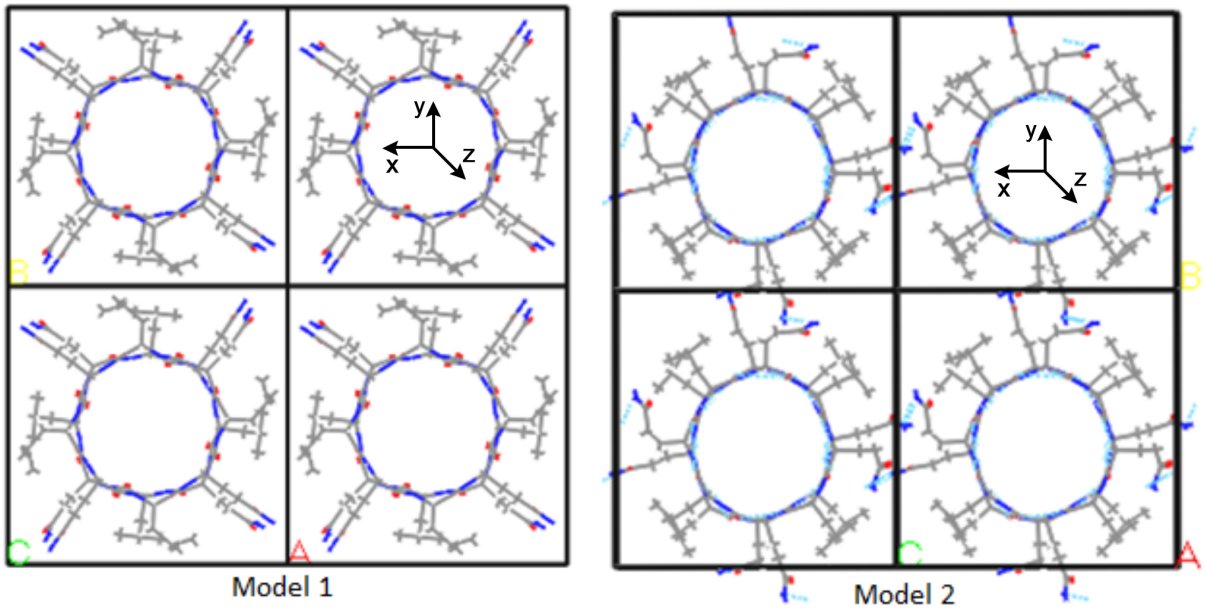

Figure S4: The structures for Model 1 and Model 2.

By rotating the cyclic peptide along z-axis, another conformer is found. (As shown in Figure S4). The lattice constants are calculated as a= 17.94 Å b= 18.11 Å c= 9.92 Å at the optimized structure. This conformer of cyclic peptide nanotubes is classified as anisotropic due to the differences in the mechanical properties along x and *y* direction. For example, the elastic constant C11 is 4.43 GPa for x direction and 1.36 for y direction. Along z direction, the interaction is comparatively weaker due to a smaller elastic constant C33 of 20.21 GPa than that

of Model 1. The total energy of Model 2 is calculated to be 67.6 kcal/mol higher than that of Model 1.

Figure S5:

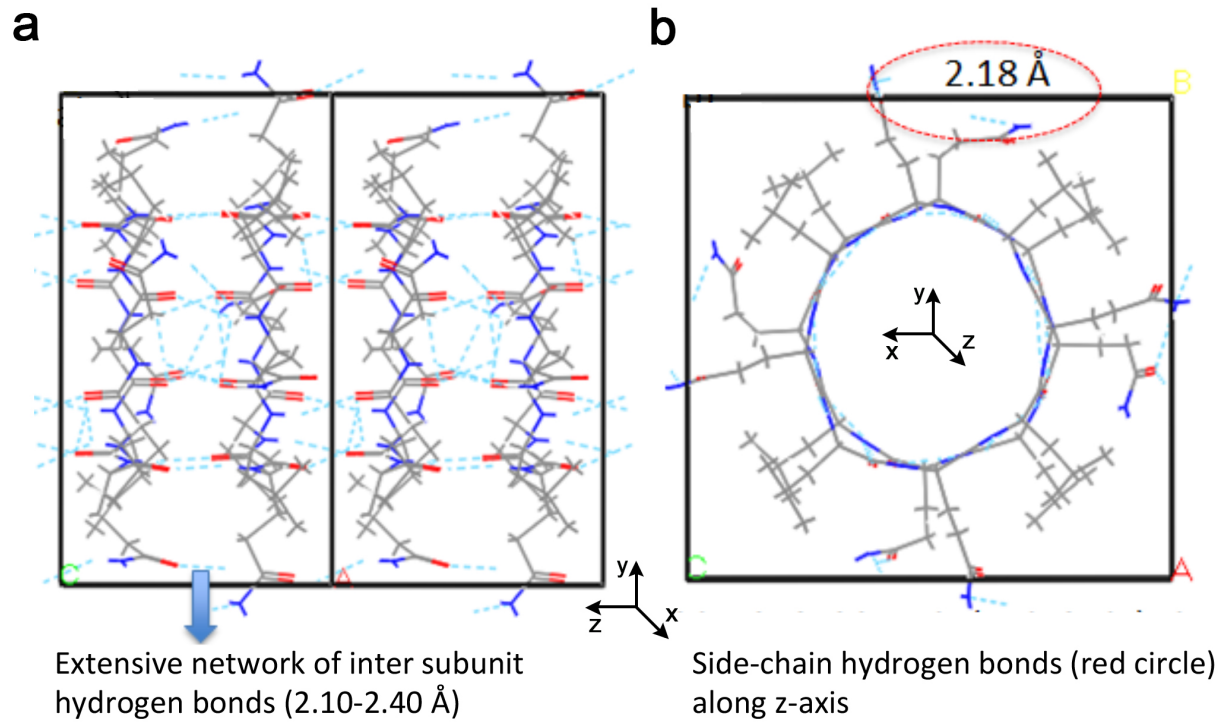

Figure S5: The hygrogen bonds between the backbones (a) and sidechains (b) in the Peptide nanostructures (Model 2)

The reason why Model 2 is higher in energy can be explained by weakening hydrogen bonds along z-axis. As shown in Figure S5, in Model 2, the inter subunit hbonds increased by about 0.2 Å for each hydrogen bond. The side chain hydrogen bonds increase by 0.2 Å for each hydrogen bond. This is also consistent with the longer lattice constant c of 9.92 Å for Model 2 compared with the more compact model1 (c=9.62 Å).

Figure S6:

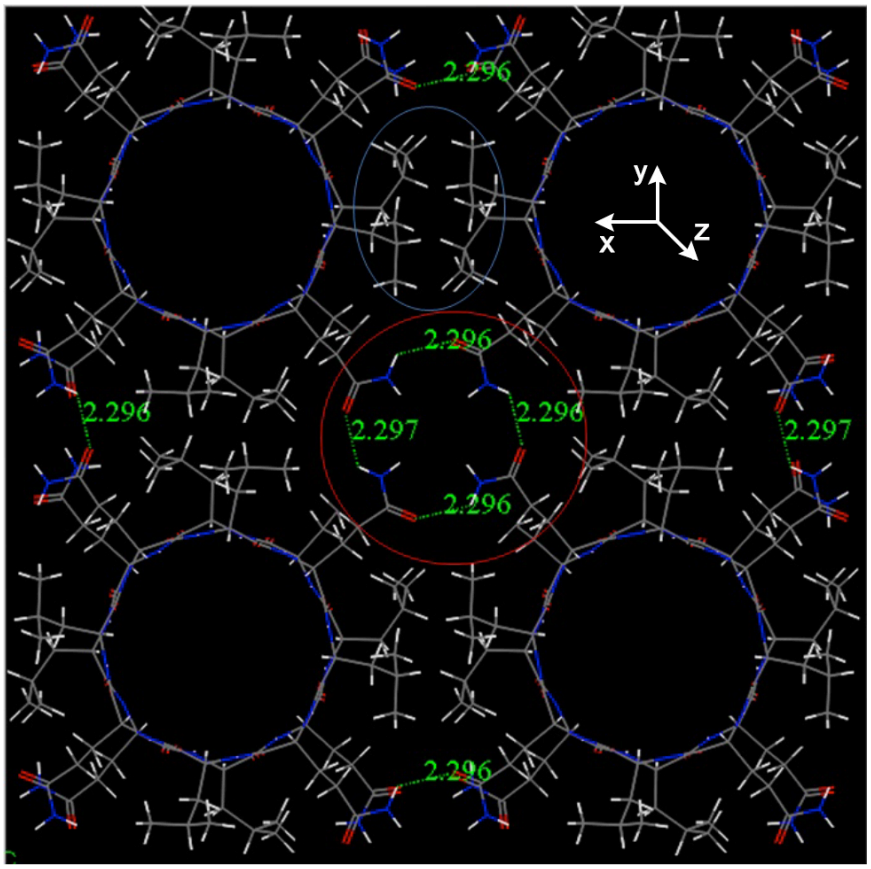

Figure S6: The lateral packing of QL4 tubes in a fiber. QL4 fibers are stabilized by interlocking hydrogen bonds and van der Waals interactions. In the ideal structure, glutamine sidechains point towards the center of the unit cell, creating two hydrogen bonds with its neighbors (red circle). Meanwhile, leucine residues are packed tightly together between each pair of tubes, allowing for close contact and favorable van der Waals interactions (blue circle).

Figure S7:

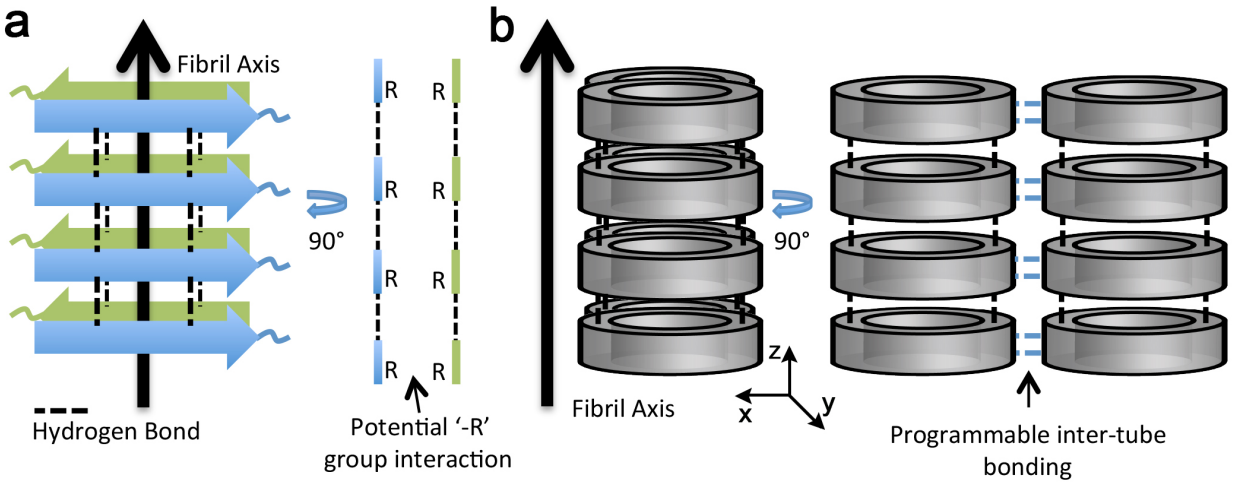

Figure S7: Simplified schematic diagram of an amyloid fibril and a DLCP assembly. (a) A typical amyloid fibril assembles by *β*–sheet formation orthogonal to the principle axis of the fiber. These sheets then bundle together such that side chains may or may not interact in the space between. Often these interactions are hydrophobic in nature and mediated by aromatic amino acids such as phenylalanine. (b) DLCP structures also assemble through backbone β–sheet-like hydrogen bonding. The side chains of the DLCP monomer may be tuned such that specific interactions can occur between individual tubes. For example, a QL4 fiber is stabilized by interlocking hydrogen bonds and hydrophobic interactions as described in Figure S6, creating a very stabile, solvent resistant structure.

Figure S8:

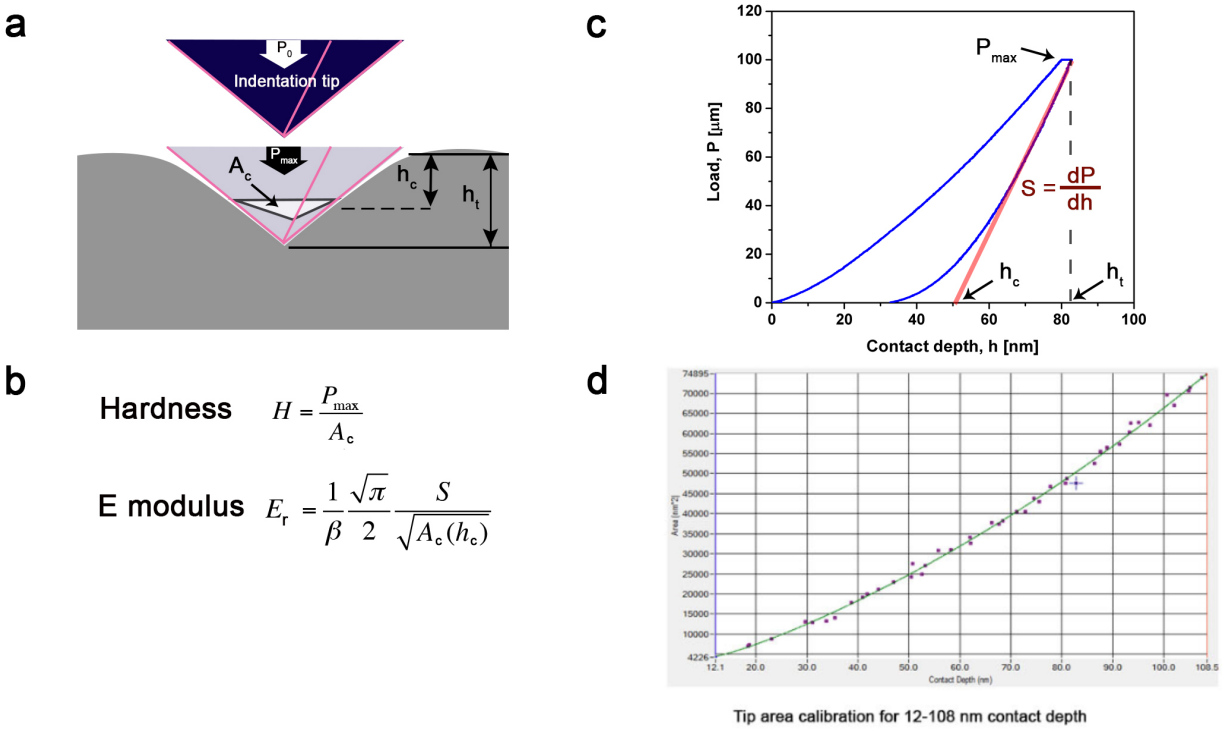

Figure S8: Nanoindentation of QL4 fibers. (a) A schematic representation of a single indent depicting the loaded and unloaded surface. Elastic energy stored in the material is responsible for the surface recoil and is used to calculate the elastic modulus. (b) Calculation of the hardness and the elastic modulus (stiffness) of a QL4 fiber. (c) A load versus depth curve from an individual indent. As the tip is withdrawn, the slope of the resulting curve (*dP/dh*) is used to calculate the material stiffness. (d) In order to process the data, a standard curve was created in which depths of 12-100 nm were probed and the corresponding indent-area was calculated.

Figure S9:

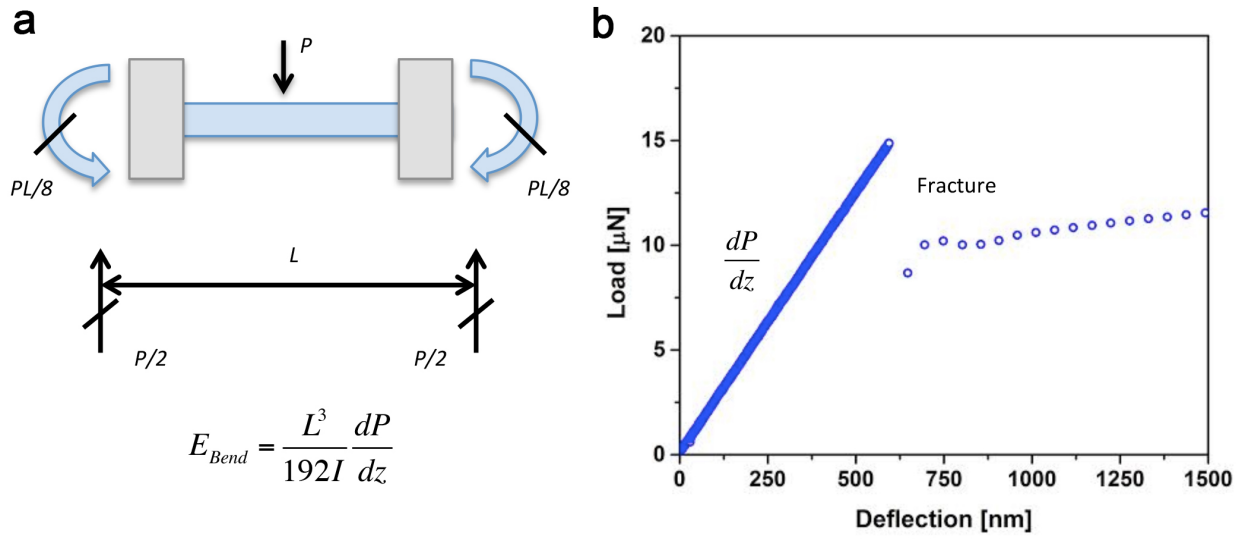

Figures S9: Bending analysis of QL4 fibers. (a) Schematic representation of a cylindrical clamped beam in bending. (b) A load versus deflection curve of an individual bending experiment highlighting the initial slope and fracture of a single fiber.

Figure S10:

Material	Elastic modulus [GPa]	Density [$mg.m^{-3}$]	Strength [GPa]	Method	Reference
QL4 fibers	~ 11	-	-	Nanoindentation	Current study
	~ 11		~ 0.1	Bending	
	~ 22 [Z direction]	~ 1	-	Simulation	
	~ 3 [X,Y directions]		-		
Diphenylalanine nanotubes	~ 19	-	-	AFM-based indentation	[5]
Collagen	1.2-7	~ 1.5	0.03-0.3	Bending (AFM)	[6, 7]
Dragline silk	~ 10	-	~ 1	Tensile	[8]
Amyloid fibrils	0.2-14	-	0.1-1	Bending/tensile (AFM)	[9, 10]
Suckerin	~ 7 [Dry]	-	-	Nanoindentation	[11, 12]

Figures S10: Tabulated modulus, strength, and density values used to create the Ashby plots in Figure 7.

References:

1. Hartgerink, J.; Granja, J.; Milligan, R.; Ghadiri, M., Self-Assembling Peptide Nanotubes. *J. Am. Chem. Soc* **1996,** *118*, 43-50.
2. Movasaghi, Z.; Rehman, S.; Rehman, I. U., Raman Spectroscopy of Biological Tissues. *Applied Spectroscopy Reviews* **2007,** *42*, 493-541.
3. Sun, H., COMPASS: An Ab Initio Force-Field Optimized for Condensed-Phase Applications Overview with Details on Alkane and Benzene Compounds. *The Journal of Physical Chemistry B* **1998,** *102*, 7338-7364.
4. Carvajal Diaz, J. A.; Çağin, T., Thermo-Mechanical Stability and Strength of Peptide Nanostructures from Molecular Dynamics: Self-assembled Cyclic Peptide Nanotubes. *Nanotechnology* **2010,** *21*, 115703.
5. Kol, N.; Adler-Abramovich, L.; Barlam, D.; Shneck, R. Z.; Gazit, E.; Rousso, I., Self-assembled Peptide Nanotubes are Uniquely Rigid Bioinspired Supramolecular Structures. *Nano Lett.* **2005,** *5*, 1343-1346.
6. Yang, L., et al., Micromechanical bending of single collagen fibrils using atomic force microscopy. *Journal of Biomedical Materials Research Part A*, **2007**. *82A*, 160-168.
7. Shen, Z.L., et al., Stress-Strain Experiments on Individual Collagen Fibrils. *Biophysical Journal*, **2008**, 95, 3956-3963.
8. *Gosline, J.M., Guerette, P.A., Ortlepp, C.S. & Savage, K.N.* The mechanical design of spider silks: from fibroins sequence to mechanical function. *Journal of Experimental Biology* **1999** *202, 3295–3303.*
9. Knowles, T. P. J.; Buehler, M. J., Nanomechanics of Functional and Pathological Amyloid Materials. *Nat. Nanotech.* **2011,** *6*, 469-479.
10. Adamcik, J.; Lara, C.; Usov, I.; Jeong, J. S.; Ruggeri, F. S.; Dietler, G.; Lashuel, H. A.; Hamley, I. W.; Mezzenga, R., Measurement of Intrinsic Properties of Amyloid Fibrils by the Peak Force QNM Method. *Nanoscale* **2012,** *4*, 4426-4429.
11. Guerette, P. A.; Hoon, S.; Ding, D.; Amini, S.; Masic, A.; Ravi, V.; Venkatesh, B.; Weaver, J. C.; Miserez, A., Nanoconfined β-sheets Mechanically Reinforce the Supra-Biomolecular Network of Robust Squid Sucker Ring Teeth. *ACS Nano* **2014,** *8*, 7170-7179.
12. Guerette, P. A.; Hoon, S.; Seow, Y.; Raida, M.; Masic, A.; Wong, F. T.; Ho, V. H. B.; Kong, K. W.; Demirel, M. C.; Pena-Francesch, A.; *et al.*, Accelerating the Design of Biomimetic Materials by Integrating RNA-Seq with Proteomics and Materials Science. *Nat. Biotech.* **2013,** *31*, 908-915.